




## Research Article

# Least Square Estimation-Based Different Fast Fading Channel Models in MIMO-OFDM Systems

Walaa Hussein <sup>1,2,3</sup> Kamil Audah,<sup>1,2,3</sup> N. K. Noordin <sup>1,2</sup> Habib Kraiem,<sup>4</sup>  
Aymen Flah <sup>5,6,7,8</sup> Mohd Fadlee,<sup>1,2</sup> and Alyani Ismail<sup>1,2</sup>

<sup>1</sup>Department of Computer and Communication Systems Engineering, Faculty of Engineering, Universiti Putra Malaysia, Serdang, Selangor 43400, Malaysia

<sup>2</sup>Wireless and Photonics Networks Research Centre of Excellence (WiPNET), Faculty of Engineering, Universiti Putra Malaysia, Serdang, Selangor 43400, Malaysia

<sup>3</sup>Department of Computer Technology Engineering, Faculty of Engineering, Iraq University College, Basra, Iraq

<sup>4</sup>Department of Electrical Engineering, College of Engineering, Northern Border University, Arar, Saudi Arabia

<sup>5</sup>College of Engineering, University of Business and Technology (UBT), Jeddah 21448, Saudi Arabia

<sup>6</sup>MEU Research Unit, Middle East University, Amman, Jordan

<sup>7</sup>The Private Higher School of Applied Sciences and Technology of Gabes, University of Gabes, Gabes, Tunisia

<sup>8</sup>National Engineering School of Gabes, University of Gabes, Gabes 6029, Tunisia

Correspondence should be addressed to Walaa Hussein; [gs60014@student.upm.edu.my](mailto:gs60014@student.upm.edu.my) and N. K. Noordin; [nknordin@upm.edu.my](mailto:nknordin@upm.edu.my)

Received 7 April 2023; Revised 13 July 2023; Accepted 28 July 2023; Published 29 August 2023

Academic Editor: B. Rajanarayan Prusty

Copyright © 2023 Walaa Hussein et al. This is an open access article distributed under the Creative Commons Attribution License, which permits unrestricted use, distribution, and reproduction in any medium, provided the original work is properly cited.

In cellular wireless communication systems, channel estimation (CE) plays a pivotal role as a crucial technique applied in orthogonal frequency division multiplexing (OFDM) modulation. CE utilizes a variety of methods, including decision-directed channel estimation, pilot-assisted channel estimation (PACE), and blind channel estimation. Among these options, PACE is widely favored for its remarkable stability and consistent superior performance. The idea of massive multiple-input multiple-output (MIMO) shows tremendous potential for the future of wireless communications. However, existing massive MIMO systems face challenges with their high computational complexity and intricate spatial structures, preventing efficient utilization of channel and sparsity features in these multiantenna systems. In communication channels, the signal received is often influenced by the characteristics of the channel and noise present at the receiver. To address this issue, an efficient dataset is utilized, employing the least square (LS) algorithm for minimization. OFDM is a commonly and widely used modulation method in communication systems utilized to specifically combat resonance fading in wireless channels. In wireless communication systems employing OFDM-MIMO, frequency selectivity and time-varying attributes due to multipath channels cause Inter-carrier Interference (ICI) among symbols. Channel estimation is a vital aspect for mitigating the effects of fading channels. This investigation focuses on the application of a method examined in the study, which involves a block-type pilot symbol-assisted estimation technique for Rayleigh and Rician fading channel models. The research assesses the performance of the least square (LS) channel estimators in fast-fading channel models while employing various symbol mapping techniques focusing on bit error rate, throughput, and mean square error. The results indicate that the LS estimator exhibits excellent performance in Rayleigh and AWGN channels within the pedestrian A (PedA) model for both uplink and downlink scenarios. It outperforms the PedA model without channel estimation.

## 1. Introduction

MIMO-OFDM technology is a significant advancement that optimizes time, frequency, and spatial dimensions, resulting in substantial improvements in spectral efficiency, power

efficiency, and transmission rate in communication systems. This technology plays a crucial role in wireless broadband communication systems. To fully harness the potential of MIMO-OFDM, precise channel state information (CSI) is vital and can be achieved through channel estimation.

Channel estimation serves as the foundation for various functionalities, including precoding, signal detection, resource allocation, indoor positioning, and physical layer security. Channel estimation can be categorized into two methods: blind channel estimation and pilot-based channel estimation. The choice between these methods determines the approach used. In blind channel estimation, summary statistics, such as second-order or high-order statistics, from the received signal are utilized to estimate the channel without requiring dedicated pilot signals. On the other hand, pilot-based channel estimation relies on dedicated pilot signals to perform the estimation [1]. In [2], the authors introduce a blind channel estimation method that utilizes statistical information related to the received signal's average power. This approach converts the average estimation into a quadratic equation that incorporates the channel gain, providing a way for user terminals to estimate the downlink channel gain in MIMO systems without requiring dedicated downlink pilot resources. Nevertheless, it should be emphasized that this method is tailored for time division duplex (TDD) systems and does not take advantage of sparse channel characteristics, potentially leading to suboptimal estimation accuracy.

In [3], researchers present an alternative blind channel estimation technique tailored for massive MIMO systems, leveraging the expectation profit-maximizing (EM) algorithm. Utilizing the sparseness of the channel in the angular domain, this method improves channel estimation precision. Although the EM-based approach offers improved accuracy, it comes with the drawback of being computationally intensive, potentially posing challenges in real-world implementations. The benefits of blind channel estimation include low dependence on known parameters and excellent spectral efficiency. It is more complex and has reduced real-time performance, among other drawbacks, including less accurate channel estimates. However, in pilot-based channel estimation, pilot symbols are included in transmissions so that the receiver can make channel estimates based on the pilot signals it receives. In [4], in comparison to blind channel estimation, this method does reduce spectral efficiency, but it is often preferred due to its ease of use. LS as well as MMSE methods are common methods of pilot-based techniques. Despite using a relatively straightforward method of interpolation, the LS algorithm's performance is hindered by poor attention to noise.

MMSE algorithm provides enhanced estimation accuracy when compared to LS methods. The MMSE algorithm provides better estimation accuracy because it takes into account the full channel statistical data and noise variance. In spite of this, it emphasizes inverting the channel correlation matrix, which adds a significant amount of complexity to the computation and necessarily requires having prior channel statistics. To address this issue, the authors in [5–7] propose ALMMSE, a linearized version of MMSE that is optimized for fast-fading channels. The ALMMSE technique reduces complexity by filtering and minimizing correlation matrices. Many channel parameters must be estimated in MIMO-OFDM systems because of the extremely high density of transceiver antenna pairs and the large number of

subcarrier channels involved. Traditional pilot-based channel estimation methods, on the other hand, reduce spectral efficiency and increase system complexity, making them impractical for use in massive MIMO systems. To address this challenge, researchers have put forth time-domain sparse channel estimation algorithms, particularly compressed sensing (CS) algorithms. CS offers the advantage of concurrently estimating relevant tap positions and their corresponding channel coefficients, making it a preferred choice as it requires fewer pilots while achieving superior estimation performance. The success of the CS-based reconstruction algorithm for MIMO-OFDM channel estimation depends on the pilot positions, which in turn affect the recovery matrix. Traditional algorithms struggle to fully exploit the block-sparse essence of the channel to jointly maximize pilot locations and symbols for precise reconstruction, despite progress in the study of massive MIMO-OFDM channels. Existing optimization methods, which heavily rely on ideal assumptions and model approximations, may encounter limitations in handling more complex scenarios. To overcome this challenge, a promising and efficient approach involves using deep learning-based channel estimation. Deep learning leverages offline big data training and online real-time data updating, enabling more robust and adaptive channel estimation in dynamic and evolving wireless environments [8].

Deep learning demonstrates remarkable capabilities in extracting features and performing nonlinear mapping, thereby offering substantial enhancements to channel estimation performance in difficult scenarios. The goal is to strike a balance between the high complexity of online testing and the complexity of offline training, leading to enhanced operational efficiency. In tackling Inter-carrier Interference (ICI) mitigation, the authors in [9] introduce a distinctive pilot pattern and channel estimation approach. This design combines comb-type and clustered patterns, effectively mitigating ICI while minimizing the pilot density. However, this method involves FFT operations and an iterative procedure for data extraction, as well as identifying the most important routes of the channel impulse response (CIR), making it mathematically complex. Another approach, iterative interference cancellation [10–15], has been extensively studied to exploit enhancing performance by considering the temporal variation of the time-varying channel. The disadvantage of this approach is its increased computational complexity when compared to linear equalizers like MMSE and LS.

In conclusion, the self-mitigation of Inter-carrier Interference (ICI) has become a highly promising strategy, attracting considerable research attention in recent times. Certain studies [16–18] have explored applying a time-domain window to the received OFDM signals, leading to the concentration of ICI power on the principal diagonal of the coupling matrix. In addition, a recent innovative approach introduced in [19, 20] involves adaptive windowing, achieving its goals with linear complexity. This technique directly monitors an ideal receiver window to optimize the average SNR.

The key findings and contribution of this research can be outlined as follows:

- (1) A MIMO-OFDM system has been devised, tailored for 5G and future communication systems, utilizing the pedestrian A channel profile model to account for mobility and frequency selective fading effects. The design assumes that the receiver lacks knowledge of instantaneous channels, necessitating the inclusion of pilot signals in the transmitted data symbols for channel estimation.
- (2) Modeling the channel time-frequency response by generating a new dataset with 5G specifications as a 2D image using the PedA model using the MATLAB simulator [21]. This research article proposes a new scenario with 5G specifications to generate 40000 frames. Each frame consisted of four 2D images formed as time-frequency responses with different models for channels experiencing rapid changes in signal strength or fading. In MIMO-OFDM such as AWGN, Rayleigh, and Rician channels with 64-QAM modulation techniques using the PedA model. This is for the objective to generate noisy channels by the least square channel estimation method with a diamond pilot pattern design for the uplink and downlink.
- (3) Studying the performance of OFDM-MIMO uplink/downlink systems without channel estimation to explore various fast-fading channel models, including Additive white Gaussian noise, Rician channel, and Rayleigh channel while implementing 64-QAM modulation techniques.
- (4) The performance of the LS channel estimation method has been assessed by comparing the bit error rate (BER) and mean square error (MSE) for different modulation schemes, including 64-QAM, 256-QAM, and 1024-QAM, in AWGN, Rayleigh, and Rician channels.

The structure of this paper is as follows: In Section 2, a comprehensive review of the relevant literature is provided. Section 3 explains the OFDM system, while Section 4 explores multipath fading channels. State-of-the-art channel estimators, including LS for fast fading, are discussed in Section 5. Section 6 presents the proposed system model for the fast-fading channel estimator. The channel model is described in Section 7, and in Section 8, the performance of the channel estimators is evaluated in terms of physical layer data throughput and mean square error (MSE). Finally, the paper is concluded in Section 9.

## 2. Related Works

Several methods have been developed to estimate the channel variance in OFDM systems, either across multiple OFDM symbols or within a single OFDM signal. Most of these approaches are based on pilot symbols [22–24]. In situations where channels experience rapid changes, a significant number of unknown channel coefficients need

estimation due to the high-order variations observed within a single OFDM symbol cycle [25, 26]. Several approaches have been put forward to address this, such as the base development model (BDM) [27, 28], block-sparse Bayesian learning (BSBL) [29, 30], and the piecewise linear model (PLM) [31, 32], aimed at reducing the number of coefficients that require estimation, which approximate the channel variation.

This study proposes the use of the least square (LS) technique for channel variance estimation in multipath fading channel OFDM-MIMO systems. The method includes zero-padding an OFDM symbol with a cyclic prefix and inserting an impulse signal among these zeros. The obtained impulse signal is used by the LS estimation method in the receiver to create a channel estimate at the OFDM symbol's pilot sample. After that, we use a linear model to predict the channel shifts over the course of an OFDM symbol.

## 3. OFDM System

Within an OFDM system, multiple-input bits are aggregated and combined to create a single data symbol. These data symbols, denoted as  $X(0)$  to  $X(N-1)$ , undergo modulation using a digital modulation technique. Subsequently, in the process of inverse fast Fourier transform (IFFT), the serial data symbols are converted into their parallel counterparts [33]. The IFFT process ensures the orthogonality of each subcarrier and maps the  $N$  data symbols onto  $N$  subcarriers. Data symbols handled by IFFT are represented by  $x(0), x(1), \dots, x(N-1)$  and mathematically expressed as [34]

$$x(n) = \frac{1}{\sqrt{N}} \sum_{k=0}^{N-1} X(k) e^{j2\pi kn/N}. \quad (1)$$

The OFDM system uses  $N$ -point IFFT samples as it is in Figure 1. For each OFDM symbol, “ $n$ ” is varying between zero (0) and  $(N-1)$  and  $x(n)$  represents the  $n^{\text{th}}$  sample. Each OFDM symbol is comprised of  $N$  IFFT samples. However, when these symbols meet the multipath channel, they are overcomplicated with channel taps, resulting in the presence of OFDM symbol samples from the preceding symbol. This occurrence results in Interblock Interference (IBI). In order to counter IBI, a longer cyclic prefix than the number of channel taps ( $L$ ) is added to the commencement of each OFDM signal. The length of the cyclic prefix ( $G$ ) needs to be greater than  $L$  (i.e.,  $G > L$ ). Once the cyclic prefix is added, a serial stream is generated from the parallel samples. These transmitted samples, which are received as  $x(n-G+1) \dots x(N-1)$ , are subject to AWGN. The samples received are depicted as follows [34]:

$$y(n) = x(n) \otimes h(l) + v(n). \quad (2)$$

In the context of the received signal,  $y(n)$  represents the  $n^{\text{th}}$  received sample,  $h(l)$  denotes the  $l^{\text{th}}$  channel tap, and AWGN samples are denoted by  $v(n)$ , where  $n$  is a natural number. The equation gives the receiver's expression for the FFT of the incoming signal (3):

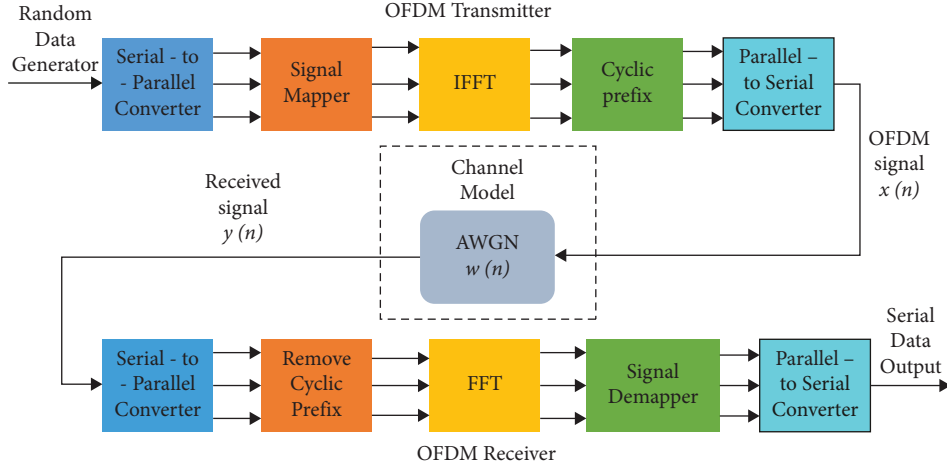


FIGURE 1: Illustration of the OFDM transmitter and receiver.

$$Y(k) = X(k)H(k) + V(k), \quad (3)$$

where  $Y(k)$ ,  $H(k)$ ,  $X(k)$ , and  $V(k)$  are  $N$ -point FFT of samples of  $y(n)$ ,  $h(n)$ ,  $x(n)$ , and  $v(n)$ , respectively, and which can be represented as follows:

$$Y(k) = \frac{1}{\sqrt{N}} \sum_{n=0}^{N-1} y(n) e^{-j2\pi kn/N}, \quad (4)$$

$$H(k) = \frac{1}{\sqrt{N}} \sum_{l=0}^{N-1} h(l) e^{-j2\pi kn/N}.$$

In this case,  $H(k)$  represents the fast Fourier transform (FFT) of  $h(l)$ , which is achieved through zero padding of  $h(l)$ .

$$X(k) = \frac{1}{\sqrt{N}} \sum_{n=0}^{N-1} x(n) e^{-j2\pi kn/N}, \quad (5)$$

$$V(k) = \frac{1}{\sqrt{N}} \sum_{n=0}^{N-1} v(n) e^{-j2\pi kn/N}.$$

#### 4. Channels with Multipath Fading

In mobile radio channels, there are two distinct types of fading: large and small. Because the structure of the received signal follows a Rayleigh or Rician probability distribution in situations with a large number of reflective paths, small-scale fading is also known by these names (R-PDF).

Rayleigh fading occurs in situations with numerous diverse reflective paths and the absence of a strong line-of-sight (LOS) propagation path. On the other hand, Rician fading occurs when a dominant LOS path exists alongside multipath components. The multipath channel can be accurately represented using equation (6) [34].

$$h = \sum_{l=0}^{L-1} a_l e^{-j2\pi F_c \tau_l}. \quad (6)$$

In this context,  $a_s$  represents the  $l$ th attenuation factor,  $v_s$  denotes the  $l$ th delay factor, and  $F_c$  stands for the carrier frequency.

$$h = \sum_{l=0}^{L-1} \overbrace{a_l \cos(j2\pi F_c \tau_l)}^p - j \left( \sum_{l=0}^{L-1} \overbrace{a_l \sin(j2\pi F_c \tau_l)}^{-q} \right). \quad (7)$$

Real and imaginary Gaussian random variables ( $p$  and  $q$ ) can be represented by the following formula:

$$p = \sum_{l=0}^{L-1} a_l \cos(j2\pi F_c \tau_l), \quad (8)$$

$$q = - \sum_{l=0}^{L-1} a_l \sin(j2\pi F_c \tau_l).$$

If  $L \rightarrow \infty$ , subsequently, the central limit theorem is introduced in equation (8).

$$\lim_{L \rightarrow \infty} h = \lim_{L \rightarrow \infty} \sum_{l=0}^{L-1} a_l e^{-j2\pi F_c \tau_l}. \quad (9)$$

As a result, the CDF can be expressed in the following manner:

$$F_R(r) = \iint \frac{1}{\sqrt{2\pi\sigma h^2}} e^{-(p^2+q^2)/(2\sigma h)^2} dP dQ. \quad (10)$$

The importance of the variance of channel coefficients, denoted as  $(\sigma h)^2$ , lies in its significant influence on the probability density function, which can be mathematically represented by equation (11).

$$f_R(r) = \frac{r}{(\sigma h)^2} e^{-(p^2+q^2)/(2\sigma h)^2} = \frac{r}{(\sigma h)^2} e^{-(r^2)/(2\sigma h)^2}. \quad (11)$$

Afterward, the Rician probability density function, which accounts for the existence of a LOS path, is precisely defined by equation (12).

$$f_R(r) = \frac{r}{(\sigma h)^2} e^{-(p^2+q^2)/(2\sigma h)^2} I_0\left(\frac{rA}{(\sigma h)^2}\right). \quad (12)$$

Here, the Bessel function is denoted by  $I_0$ , where  $A$  is the LOS path amplitude.

In order to model the impacts of electromagnetic data transmission, fading channel models are prevalent in cellular networks and broadcast communication, as well as being employed in underwater acoustic communications to mimic the effects of water distortion. Figure 2 shows the basic block diagram of the proposed multipath fading channel model. The input signal undergoes two separate amplification stages: one with a constant gain and the other with a variable gain. The amplitude of a signal transmitted through a communication channel is assumed to undergo random variations or fading, following a Rayleigh distribution [35].

$$y(t) = g_1 \cdot s(t) + 0.5 (\tau \cdot g_2 \cdot s(t)) + 0.25 (\tau \cdot g_2 \cdot s(t)) + n(t). \quad (13)$$

In the given context,  $y(t)$  denotes the output signal,  $s(t)$  represents the input signal,  $\tau$  refers to the delay or phase shift,  $g_1$  stands for the constant gain,  $g_2$  represents the variable gain, and  $n(t)$  represents the impact of noise; a statistical model is employed to simulate the influence of a radio signal's propagation environment on wireless devices. To generate noise, the following equation code was used, as indicated in equation (14) [35].

$$y = \text{AWGN}(x, \text{SNR}, \text{'measured'}). \quad (14)$$

The  $x$ -vector signal is corrupted with white Gaussian noise, congratulations to this function. The SNR (signal-to-noise ratio) is a scalar value in decibels that represents this signal-to-noise ratio. Complex noise is introduced by the AWGN when  $x$  is a complex signal. In this syntax, the function measures the power of  $x$  before adding noise, assuming that  $x$ 's power is 0. The level of noise in a channel is typically measured using a number of different metrics.

- (1) Signal-to-noise ratio per sample
- (2) The ratio of bit energy to the noise power spectral density, denoted as  $E_b/N_0$
- (3) The ratio of symbol energy to the noise power per unit bandwidth, denoted as  $E_s/N_0$

The BER represents the proportion of incorrectly received bits to the total number of transmitted bits within a defined duration. SNR or S/N represents the signal's power in relation to the noise affecting it. In simpler terms, it quantifies the strength of the desired signal (e.g., music) relative to the background noise level. A higher SNR implies that the background noise is less perceptible. This mathematical relationship is expressed in equation (15) [35].

$$\text{SNR} = \left(\frac{P_{\text{signal}}}{P_{\text{noise}}}\right) = \left(\frac{A_{\text{signal}}}{A_{\text{noise}}}\right)^2. \quad (15)$$

After analyzing the influence of the bit error rate (BER) on signal-to-noise ratio (SNR), the outcomes demonstrate

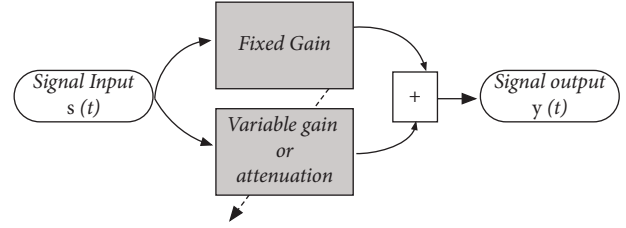


FIGURE 2: Structure of a channel affected by multipath fading.

a significant enhancement in BER performance at low SNR levels, whereas no significant improvement is observed at high SNR levels. At low SNR, the dominant factor affecting the BER is white Gaussian noise, which can be reduced by increasing SNR. However, at high SNR, the primary contributor to the BER is phase estimation error, and simply raising SNR does not lead to improvement. Consequently, flat fading channels exhibit poorer BER performance compared to frequency selective fading channels, while AWGN channels show the highest BER performance. To simulate the channel's physical processes impacting the transmitted signal, it is possible to create a physically realistic channel model. For instance, in wireless communications, channel simulation involves calculating the reflections from objects present in the environment. The “scatterplot ( $x$ )” function generates a scatter plot for the signal  $x$ . If  $x$  is a complex vector, the real and imaginary components will be displayed as phase and quadrature, respectively, in the scatter plot. However, if  $x$  is a real vector, the scatter plot displays it as such, without trying to figure out what its phase and quadrature components are.

## 5. Channel Estimation

Communication systems frequently are using OFDM to mitigate frequency-selective fading in wireless channels. The received signal in such channels is affected by the channel itself. To effectively retrieve the transmitted symbols, it becomes crucial to estimate and compensate for the channel effects at the receiver. This is typically achieved by utilizing specific symbols known as pilots; for accurate channel estimation, the transmitter and the receiver use the time-frequency coordinates and values already in their possession. Three different structures of pilot symbol arrangements are taken into consideration, which include block-type, comb-type, and lattice-type, as described in [36]. In the block-type arrangement, in the beginning, the symbols of the pilot are transmitted to an OFDM block across all subcarriers. In contrast, the comb-type arrangement entails the inclusion of pilots in specific subcarriers of a few OFDM symbols. The lattice-type arrangement involves the insertion of pilots along both time and frequency axes, forming a diamond-shaped constellation with predefined periods [37].

To infer the unknown channel response values, traditional pilot-based techniques like LS and MMSE rely on the pilot values situated within time-frequency grids. These methods have been fine-tuned and optimized for diverse scenarios [38]. Unlike LS estimation, which operates without any prior knowledge of the channel's statistics, MMSE estimation achieves superior performance by taking advantage

of the channel's statistics and noise variance. In practical scenarios, several techniques have been suggested to implement MMSE while reducing the complexity of the scheme. These techniques involve using estimates of channel statistics instead of precise data. Figure 3 illustrates a common block-type pilot layout, where multiple pilot symbols are sent over multiple OFDM symbols simultaneously. Both LS and MMSE methods can be used to estimate the block-type pilot configuration [39].

Least square (LS) estimation is a typical technique for pilot-based channel estimation since it delivers acceptable performance with moderate complexity. Minimizing the squared difference between the transmitted and received signals is the goal of the channel least square estimator. Equation (2) demonstrates that the provided equation (6) can be utilized to compute the LS of the channel at the pilot subcarriers:

$$\hat{h}_p^{\text{LS}} = \operatorname{argmin} \|y_p - X_p \hat{h}_p\|_2^2 = X_p^{-1} y_p. \quad (16)$$

For positions without pilot symbols, the channel coefficients are determined through two-dimensional interpolations. In this study, linear interpolation is employed. The LS channel estimator offers the advantage of low complexity and does not necessitate knowledge of the channel and noise statistics. Taking into account, block fading assumptions make the LS channel estimator even simpler. At first, pilot symbol time-frequency grid positions are used to estimate channels with equation (3). The channel estimating for pilot positions at different time instances are averaged, assuming the channel remains unchanged during the transmission of a single subframe. Afterward, one-dimensional interpolation (specifically, linear interpolation in this case) is utilized to find the missing channel coefficients in the frequency domain [40–42].

## 6. System Model

This section describes a MIMO-OFDM system where signals are transmitted from a transmitter to a receiver. The MIMO channel model for the 5G communication system is constructed with  $N_T$  transmitter antennas and  $N_R$  receiver antennas, forming an  $N_T \times N_R$  antenna array configuration.

**6.1. Transmitter.** The transmitter processes the binary data through the modulation block, where it encodes and maps it using quadrature amplitude modulation (QAM). Assuming the system transmits information in  $T$  time slots, the QAM symbols for each time slot ( $t=1, \dots, T$ ) are combined to form a data vector, denoted as  $x(t') \in \mathbb{C}^N$ , following the description in [43].

$$x(t) = [x_1(t), x_2(t), \dots, x_N(t)], \quad (17)$$

where  $N$  denotes the total number of modulation symbols. After encoding, the data are divided into  $N_T$  vectors, corresponding to the  $N_T$  [43] transmit antennas:

$$x_i(t) = [x_i(t), x_{i+NT}(t), x_{i+2NT}(t), \dots], \quad (18)$$

$$i = 1, \dots, 2, \dots, N_T.$$

For each antenna, the information is converted from serial to parallel formats. Pilot signals, known to both the transmitter and the receiver, are then added to the data for each layer to facilitate channel estimation. The IFFT block is then applied to  $x_a(t)$  with  $a = 1, N_T$ . The signal vector with a pilot inserted into the corresponding data  $x_i(t)$  is used to transfer the signals from the frequency domain to the time domain. This transformation is represented by the notation  $\tilde{x}_a(t)$ ,  $s$  observed in [43].

$$\tilde{x}_a(t) = \text{IFFT}\{x_a(t)\}. \quad (19)$$

The CP insertion block inserts a CP of a guard interval of length  $N_G$  which is introduced to reduce intersymbol interference (ISI) after the IFFT transformation. Including the cyclic prefix enables the transmission of the signal, denoted as  $\tilde{x}_{ga}$  [43, 43], to be formulated in the time domain as follows:

$$[\tilde{x}_{ga}(t)]_n = \begin{cases} [\tilde{x}_a(t)]_{n+N_{\text{FFT}}}, & n = -N_G, -N_G + 1, \dots, -1, \\ [\tilde{x}_a(t)]_n, & n = 0, 1, \dots, N_{\text{FFT}} - 1, \end{cases} \quad (20)$$

where the signal  $\tilde{x}_a(t)$  with a length of  $N_{\text{FFT}} + N_G$  is formed by using the last  $N_G$  samples of  $\tilde{x}_a(t)$ . The last  $N_G$  samples of  $\tilde{x}_a(t)$  are utilized as a cyclic prefix and placed at the beginning of this symbol. The arrangement, which leads to the final signal format, is determined by the FFT size,  $N_{\text{FFT}}$ .

**6.2. Receiver.** Using the cyclic prefix removal module, the prefix of the cyclic could be removed from each antenna that received the signal at the receiver, providing the vector,  $\tilde{y}_b(t)$  of length  $N_{\text{FFT}}$ . According to [43], afterward, the signal is transformed into a parallel format and subjected to processing in the frequency domain using the FFT block. This process leads to the creation of a frequency-domain signal denoted as  $y_b(t)$ .

$$y_b(t) = \text{FFT}\{\tilde{y}_b(t)\}. \quad (21)$$

The pilot signal is extracted from the frequency-domain signal to estimate the channel. After obtaining the channel estimate, the received signal  $y_b(t)$  is equalized and combined into a serial sequence using the layer demapping module. The signal is then demodulated based on the transmitter's scheme. The output of the MIMO-OFDM system model comprises the final sequence of gathered binary data.

## 7. Massive MIMO Systems for 5G Communications

**7.1. Performance and Spectral Efficiency of 5G Systems.** Massive MIMO is a key technology in 5G systems that enhances performance and spectral efficiency in several ways [44]:

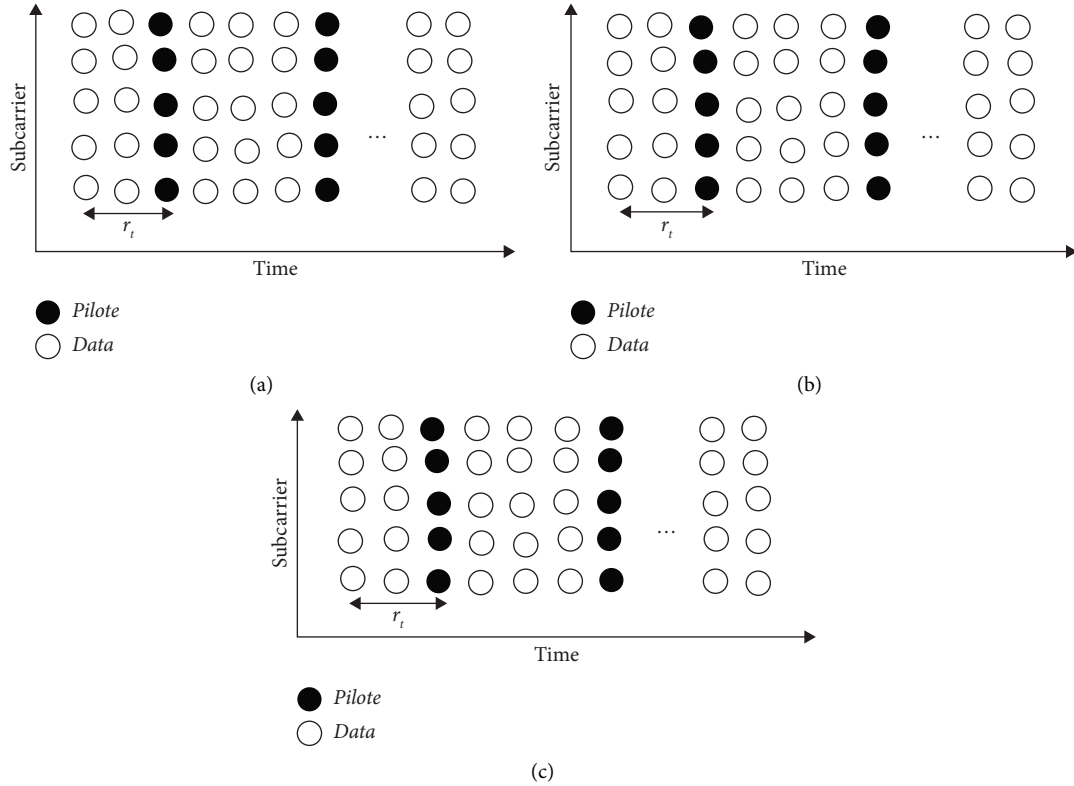


FIGURE 3: Three types of pilot pattern: (a) block, (b) comb, and (c) lattice.

- (1) **Increased spatial multiplexing:** This enables simultaneous communication with multiple user devices in the same time-frequency resource, known as spatial multiplexing. By exploiting the spatial dimension, massive MIMO significantly increases the capacity of the wireless system, allowing more users to be served simultaneously.
- (2) **Beamforming and spatial processing:** The large number of antennas in massive MIMO enables beamforming techniques, where the transmitted signals can be focused towards specific users. By steering the beams towards the intended users and nulling interference towards other directions, the signal quality at the user devices is improved. Beamforming increases the received signal strength and reduces interference, resulting in better coverage, higher data rates, and improved overall system performance.
- (3) **Interference suppression:** Massive MIMO systems can effectively suppress interference by utilizing spatial processing techniques. Since the base station has multiple antennas, it can distinguish between signals coming from different directions. By applying advanced interference suppression algorithms, massive MIMO can mitigate interference caused by other users or neighboring cells, leading to improved spectral efficiency and reduced signal degradation.
- (4) **Diversity and resilience:** Massive MIMO exploits the spatial diversity provided by a large number of antennas. This diversity improves the system's resilience to fading and interference, enhancing the overall reliability and quality of service. Even in challenging environments, where certain paths may experience deep fading, the presence of multiple antennas helps maintain reliable communication by utilizing the available strong paths.
- (5) **Energy efficiency:** Massive MIMO can also contribute to energy efficiency in 5G systems. By focusing the transmitted energy towards the intended users through beamforming, the system can reduce the overall power consumption. In addition, the ability to serve multiple users simultaneously in a single time-frequency resource improves spectral efficiency, enabling more data to be transmitted per unit of energy.
- (6) Overall, massive MIMO enhances the performance and spectral efficiency of 5G systems by increasing capacity, improving coverage, reducing interference, providing spatial diversity, and enabling energy-efficient operations. These benefits make it a fundamental technology for achieving the ambitious goals of 5G networks, such as supporting massive connectivity, high data rates, low latency, and diverse application requirements.

### 7.2. Improving Coverage and Efficiency in 5G Spectrum.

Massive MIMO utilizes beamforming techniques in order to improve the efficiency and the coverage in the 5G spectrum in the following ways [44]:

- (1) Beam steering: Massive MIMO systems utilize a significant number of antennas at the base station. By manipulating the phase and amplitude of signals transmitted from each antenna element, beamforming can direct the beams towards specific user devices. This allows the base station to focus its energy towards the intended users, improving coverage and signal quality in their direction.
- (2) Spatial multiplexing: In addition to beam steering, massive MIMO enables spatial multiplexing. It can create multiple spatially separated beams to serve multiple user devices simultaneously. This is achieved by forming different beams with different spatial characteristics, targeting different users or groups of users. Spatial multiplexing increases the capacity of the system and improves spectral efficiency, as more data can be transmitted in the same time-frequency resource.
- (3) Interference nulling: Massive MIMO beamforming can also mitigate interference. By using multiple antennas, the base station can differentiate between desired signals and interference coming from other directions. It applies adaptive beamforming techniques to suppress interference, such as nulling or canceling unwanted signals, thereby reducing interference levels and improving the signal quality at the intended receivers.
- (4) Hybrid beamforming: In practical deployments of massive MIMO, hybrid beamforming techniques are often used to strike a balance between performance and complexity. Hybrid beamforming combines digital beamforming, performed in the baseband domain, with analog beamforming, performed in the radio frequency (RF) domain. Digital beamforming is used for fine-grained beamforming adjustments and interference suppression, while analog beamforming is responsible for coarse-grained beam steering. This approach reduces the number of required RF chains, making it more practical for implementation.
- (5) Adaptive beamforming: Massive MIMO systems continuously adapt their beamforming strategies based on channel conditions, user locations, and system requirements. Through adaptive beamforming, the system optimizes the beamforming weights and beam directions to maximize the received signal quality, improve coverage, and minimize interference. Adaptive beamforming algorithms utilize channel state information (CSI) feedback from the user devices to adjust the beamforming parameters dynamically.
- (6) By utilizing beamforming techniques, massive MIMO improves coverage and efficiency in the 5G

spectrum by focusing energy towards intended users, serving multiple users simultaneously, mitigating interference, and adapting to change channel conditions. These capabilities enhance the system's capacity, data rates, and spectral efficiency, enabling better performance and user experiences in 5G networks.

## 8. Channel Model

In order to determine the channel, the signal of that pilot is separated from the signal in the frequency domain. Once the channel estimate has been obtained, the received signal  $y_{.b}(t)$  is equalized and merged using the layer demapping module, which includes all receiving antennas. The signal is then demodulated using the same method as the transmitter. The output of the MIMO-OFDM system model is the final sequence of binary data [45–47].

There are two main types of channels based on the mobility between the transmitter and the receiver: time-invariant channels and time-varying channels. A channel is considered time-invariant when both the transmitter and the receiver remain stationary in one location. There are two primary kinds of channels: time-invariant and time-varying channels, depending on the mobility between the transmitter and receiver. A channel is regarded to be time-invariant when both the transmitter and the receiver stay fixed at a single place. For example, a simple cable connection between a transmitter and a receiver or a fixed WiMAX system in which the base station and subscriber's premises equipment are immovable and are examples of time-invariant channels [48].

Communication design engineers use the basic to validate the development of transmitters and receivers; channel models like AWGN, Rayleigh, and Rician are employed. For complex communication systems, the establishment of channel models is crucial to verify the performance of the transmitter and the receiver. When building channel models, a variety of elements, various factors, such as the number of pathways, delays at each path, terrain type, Doppler frequency, and speed, are taken into consideration [49, 50].

- (1) AWGN: Additive white Gaussian noise, commonly observed in semiflex or coaxial cables connecting transmit and receive paths, as well as in space communication, is primarily associated with thermal noise in the channel. This noise may arise from electrical equipment at both the transmitter and the receiver ends [35].

$$R = \text{awgn}(T, \text{SNR}, \text{'measured'}). \quad (22)$$

In this context,  $T$  denotes the transmitted vector, while  $R$  represents the received vector, including noise, based on the signal-to-noise ratio (SNR) measured in decibels (dB).

- (2) Rayleigh: This channel type is designated for channels that lack line-of-sight (LOS) paths and do not



exhibit any dominant or LOS paths between the transmitter and the receiver.

- (3) Rician: This channel type is used for channels with both line-of-sight (LOS) and non-line of sight (non-LOS) transmission routes between the transmitter and the receiver.

Table 1 shows a comparison of three fast-fading channel models with other reference works. It is crucial to recognize that there is no universal channel model that is ideal for every scenario. The best model to use will depend on the fading environments and noise channel; the communication channel can be categorized into three types such as additive white Gaussian noise (AWGN), Rayleigh fading, and Rician fading channels. In this paper, the performance of MIMO-OFDM has been analyzed with respect to these three types of channels.

**8.1. AWGN Channel.** The AWGN channel is commonly employed in communication systems because of its non-fading nature and straightforward implementation. When signals traverse the AWGN channel, it adds white Gaussian noise to the signal [9–11]. The probability density function of the noise always follows a Gaussian distribution, which is mathematically expressed as [58]

$$f_g(x) = \frac{1}{\sigma\sqrt{2\pi}} e^{-(x-\mu)^2/2\sigma^2}. \quad (23)$$

The received signal in the AWGN channel is represented as follows, with  $x$  being a random variable,  $\mu$  denoting the mean value, and  $\sigma$  representing the standard deviation [58]:

$$r(t) = x(t) + n(t), \quad (24)$$

where  $x(t)$  = transmitted signal and  $n(t)$  = additive white Gaussian noise.

**8.2. Rayleigh Fading Channel.** In a Rayleigh fading channel, the signal passing through the channel undergoes distortion caused by the Rayleigh distribution. Multipath reception is the root cause of Rayleigh fading. The antennas receive a large number of reflected and scattered waves. The antennas receive numerous reflected and scattered waves, leading to constructive and destructive interference due to the effects of multipath. Rayleigh fading is more suitable in scenarios where there is no direct line-of-sight communication between the transmitter and the receiver [59]; the probability density function (pdf) of the Rayleigh random variable is provided by [58]:

$$p(z) = \frac{z}{\sigma^2} e^{(-z^2/2\sigma^2)}, \quad \text{for } z > 0, \quad (25)$$

where  $\sigma^2$  is the received signal's time-average power.

**8.3. Rician Fading Channel.** In a Rician fading channel, the amplitude gain follows the Rician distribution. In this type of channel, there is a line-of-sight signal path between the transmitter and the receiver. The Rician fading occurs when

one of the received signals is stronger (typically line of sight component is stronger than the other) [60, 61]. The Rician distribution is represented by the following equation [58]:

$$p(r) = \frac{r}{\sigma^2} e^{-(r^2-A^2)/2\sigma^2} I_0\left(\frac{Ar}{\sigma^2}\right) \text{ for } (A \geq 0, r \geq 0), \quad (26)$$

where  $A$  represents the peak amplitude of the dominant signal.  $I_0[\cdot]$  is the modified Bessel function.

Here are some additional information about the different fast-fading channel models:

- (1) Rayleigh fading: This is the most common fast-fading channel model. It is a good model for channels that are subject to a large number of uncorrelated multipath reflections.
- (2) Rician fading: This model is a more accurate model than Rayleigh fading for channels that have a strong direct signal component.
- (3) AWGN: This is a model for channels that are not subject to multi-path fading. It is a good model for channels that are in a laboratory setting or in a very controlled environment.

The choice of channel model will affect the design of the MIMO-OFDM system. For example, a system that uses a Rayleigh fading model will need to be more robust to signal loss than a system that uses a Rician fading model. Similarly, a system that uses an AWGN model will not need to be as robust to signal loss as a system that uses a Rayleigh fading model [22].

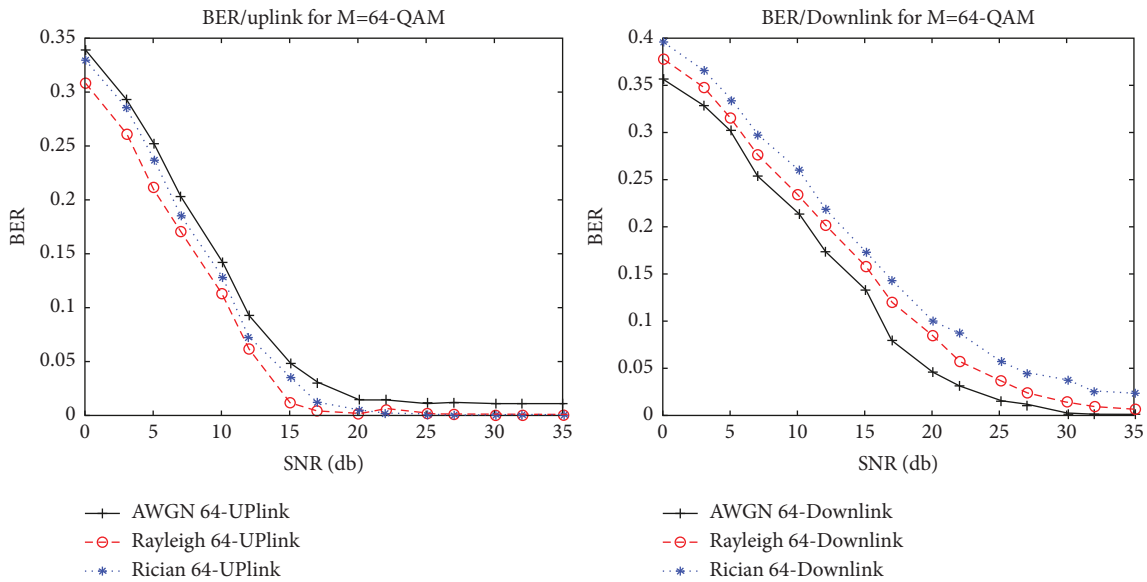
## 9. Simulation Results and Analysis

This study conducts a link-level simulation to analyze the BER for various channel models in the MIMO-OFDM system, both with and without channel estimation using LS estimators, and applying various modulation methods. Based on the 5G system's air interface standard, the simulated environment uses time-frequency resource slots with a total of 72 subcarriers (6 resource blocks (RBs) of 12 subcarriers each) and 14 OFDM symbols. The 2.1 GHz frequency, 1.6 MHz bandwidth, 1730 ns delay spread, and 50 km/h UE speed used in the experiment are all specifics of the PedA channel model under investigation. The experimental channel environment is built using the channel simulator produced at the University of Vienna [21]. The PedA channel model is subjected to noise levels ranging from 0 to 35 dB to make sure that the performance of the proposed scenario is evaluated in different signal-to-noise ratio circumstances.

Figures 4 and 5 compare the bit error rate (BER) and throughput for three distinct channel models Rician fading, Rayleigh fading, and AWGN, utilizing 64-QAM modulation and no channel estimation. Table 2 includes specific BER and the throughput for different values of SNR ranging from 0 to 35 dB. The findings reveal that the channel with no fading (AWGN) has the greatest bit error rate, while the uplink Rayleigh channel model has a lower BER and higher throughput than the Rician channel model. This is attributed

TABLE 1: Comparison of the three fast-fading channel models with other recently referenced works.

Channel model	Reference	Description
Rayleigh fading	[51]	An investigation into the performance of MIMO-OFDM systems in Rayleigh fading channels, considering varying numbers of transmit and receive antennas, as well as different modulation schemes
Rician fading	[52]	An examination of the performance of MIMO-OFDM systems in Rician fading channels, involving various Rician factor values and different antenna configurations
AWGN fading	[53]	An investigation into the performance of MIMO-OFDM systems in AWGN channels, considering different noise power levels. The findings indicate that as the noise power decreases, the performance of MIMO-OFDM systems in AWGN channels improves
Block fading	[54]	An examination of the performance of MIMO-OFDM systems in block fading channels, exploring various block lengths and employing different channel estimation techniques
Nakagami fading	[55]	An investigation into the performance of MIMO-OFDM systems in Nakagami fading channels, considering varying Nakagami parameter values and utilizing different precoding techniques
Log-normal fading	[56]	An examination of the performance of MIMO-OFDM systems in log-normal fading channels, with varying log-normal shadowing factor values, and employing different power allocation schemes
Weibull fading	[57]	A study of performance of MIMO-OFDM systems in Weibull fading channels, considering diverse Weibull shape parameter values and utilizing different diversity techniques

FIGURE 4: The performance of the bit error rate in AWGN, Rayleigh, and Rician channels without channel estimation for  $M = 64$ -QAM.

to the Rayleigh channel's presence of multiple non-line-of-sight paths, whereas the Rician channel model includes both a direct line-of-sight (LOS) signal and multiple paths. In contrast, for the nonfading downlink AWGN channels, the bit error rate is the lowest, resulting in the highest throughput. The Rayleigh channel model still exhibits a higher BER than the Rician channel model, which demonstrates a relatively lower BER.

Table 3 shows the bit error rate and throughput for LS estimator values for various SNR values in 64-QAM. The BER for 64-QAM in Table 3 shows that the AWGN-LS

channel gives lower BER, lower MSE, and higher throughput for uplink than Rayleigh and Rician fading channels. For the downlink, Rayleigh gives the best performance in terms of BER, MSE, and throughput as compared with AWGN and Rician. If we look at each value of SNR, we can notice that the bit error rate is decreased since the value of SNR increases especially when that value reaches its maximum, and of course that will be affected by the throughput value for both uplink and downlink, then that will be different when we compare those values with Table 4, where the channel is 256-QAM and we can notice that the value of SNR reaches its

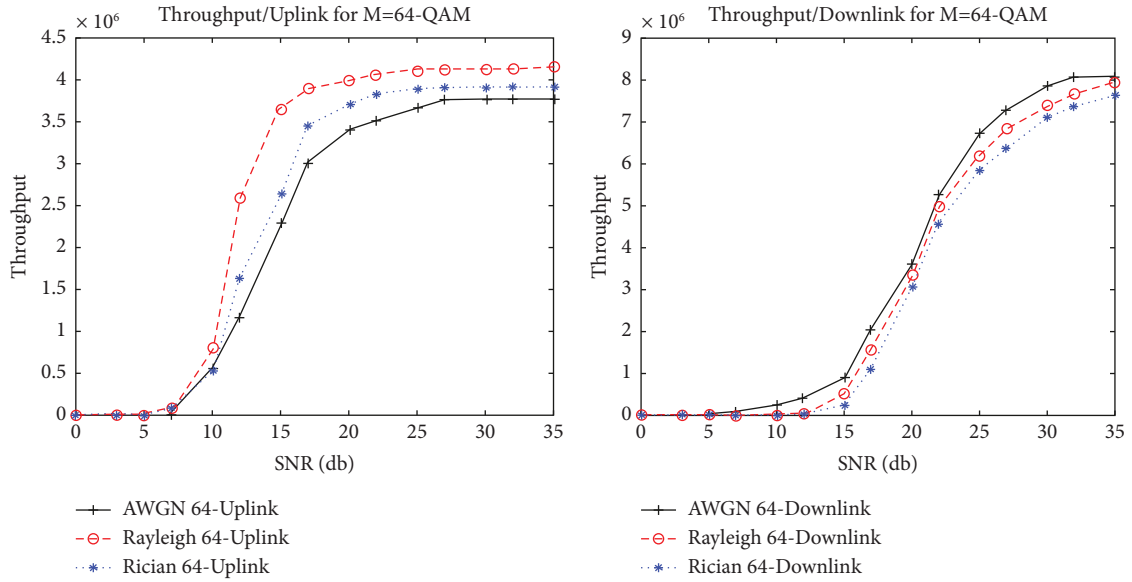


FIGURE 5: In the absence of channel estimation, the throughput performance in AWGN, Rayleigh, and Rician channels for  $M = 64$ -QAM.

TABLE 2: The configuration of parameters for the examined MIMO-OFDM system.

Parameter	Value
MIMO	$2 \times 2$
No of BS, UE	2 and 2
Simulation	Uplink/downlink
FFT size	256
Subcarrier spacing	15 kHz
Cyclic prefix	24
Type of modulation	OFDM 64, 256, and 1024-QAM
Maximum Doppler frequency	36 Hz and 200 Hz
Noise model	Gaussian noise
Sample frequency	3.84 MHz
No. of subcarriers	72
Time slot	14
Fading	AWGN, Rayleigh, and Rician
Frame structure	FDD
Channel power delay profile	Pedestrian A
Channel estimation method	Approximate-perfect and pilot-aided LS
Pilot pattern uplink/downlink	Diamond
Receiver-type MIMO	MMSE

TABLE 3: The performance of BER and throughput (both uplink and downlink) for 64-QAM without channel estimation in AWGN, Rayleigh, and Rician channels.

Channel SNR (dB)	Nonfading-AWGN						Rayleigh						Rician					
	Uplink		Downlink		Uplink		Downlink		Uplink		Downlink		Uplink		Downlink			
	BER	Throughput	BER	Throughput	BER	Throughput	BER	Throughput	BER	Throughput	BER	Throughput	BER	Throughput	BER	Throughput		
0	0.3387	0	0.3558	0	0.3079	0	0.3769	0	0.3291	0	0.3947	0	0.3291	0	0.3947	0		
3	0.2924	0	0.3268	0	0.2602	1954	0.3465	1954	0.2854	0	0.3656	0	0.2854	0	0.3656	0		
5	0.2511	0	0.3014	0	0.2109	2590	0.314	2590	0.2367	0	0.3328	0	0.2367	0	0.3328	0		
7	0.2026	1954	0.2539	102500	0.1701	84482	0.2754	84482	0.1839	58620	0.2967	58620	0.1839	58620	0.2967	58620		
10	0.1415	551028	0.2131	252500	0.1126	798270	0.2329	798270	0.1285	523672	0.259	523672	0.1285	523672	0.259	523672		
12	0.0923	1163200	0.1728	412500	0.0614	2576878	0.2005	2576878	0.0719	1617912	0.2184	1617912	0.0719	1617912	0.2184	1617912		
15	0.0486	2284796	0.1318	907750	0.0119	3649624	0.1568	3649624	0.0354	2649624	0.1717	2649624	0.0354	2649624	0.1717	2649624		
17	0.0296	3003868	0.0784	2022125	0.0041	3884328	0.1189	3884328	0.0126	3435132	0.1427	3435132	0.0126	3435132	0.1427	3435132		
20	0.0143	3389152	0.0444	3609250	0.0015	3994784	0.0839	3994784	0.005	3698922	0.0993	3698922	0.005	3698922	0.0993	3698922		
22	0.0145	3511334	0.0309	5249000	0.0048	4049380	0.0563	4049380	0.0017	3827886	0.0861	3827886	0.0017	3827886	0.0861	3827886		
25	0.012	3650644	0.015	6720500	0.0018	4096276	0.0358	4096276	0.0004	3888460	0.0563	3888460	0.0004	3888460	0.0563	3888460		
27	0.0119	3755276	0.01	7281500	0.0007	4106046	0.0229	4106046	0.0001	3904092	0.044	3904092	0.0001	3904092	0.044	3904092		
30	0.0112	3758000	0.0002	7849750	0.0003	4114092	0.0133	4114092	0	3908000	0.0372	3908000	0	3908000	0.0372	3908000		
32	0.0111	3759080	0.0001	8056000	0.0001	4128000	0.0084	4128000	0	3908000	0.0245	3908000	0	3908000	0.0245	3908000		
35	0.011	3759080	0.0001	8077750	0	4138000	0.0053	4138000	0	3908000	0.0224	3908000	0	3908000	0.0224	3908000		

TABLE 4: The bit error rate (BER) and throughput (both uplink and downlink) for 64-QAM employing LS estimators in AWGN, Rayleigh, and Rician channels.

Channel SNR (dB)	AWGN-LS				Rayleigh-LS				Rician-LS			
	Uplink		Downlink		Uplink		Downlink		Uplink		Downlink	
	BER	Throughput	BER	Throughput	BER	Throughput	BER	Throughput	BER	Throughput	BER	Throughput
0	0.2639	81823.5	0.3746	0	0.3065	82650	0.357	0	0.2639	99180	0.3749	0
3	0.1715	490606.5	0.3329	0	0.2036	400770.5	0.3358	0	0.2345	354903	0.3314	0
5	0.0888	956342.5	0.284	15200.5	0.1426	908740	0.2893	23964	0.1842	858077.5	0.2999	10946
7	0.039	1319094	0.2398	249933	0.0944	1220747	0.2316	296915	0.1294	1109176	0.2552	203424
10	0.0145	1532331	0.193	927660	0.0549	1422413	0.1574	999986.5	0.08	1333984	0.2026	881477.5
12	0.0054	1600931	0.1494	1662955	0.0284	1500931	0.0925	1983901	0.0501	1414155	0.1704	1576919
15	0.0013	1641429	0.1084	2457158	0.0126	1538950	0.0484	2932721	0.0273	1438123	0.1298	2330975
17	0.0002	1650521	0.075	2848150	0.0052	1549694	0.0245	3369096	0.022	1450521	0.1107	2783060
20	0	1653000	0.044	3100741	0.0024	1552174	0.0096	3474558	0.021	1452174	0.0761	3015211
22	0.0001	1651347	0.0293	3291507	0.0008	1553000	0.0051	3495797	0.02	1453000	0.0656	3189761
25	0	1653000	0.0179	3357836	0.0003	1553000	0.0013	3496090	0.018	1453000	0.0476	3261327
27	0	1653000	0.0099	3385764	0.0001	1553000	0.0004	3492273	0.016	1453000	0.041	3277036
30	0	1653000	0.0064	3389255	0	1553000	0.0001	3499255	0.014	1453000	0.0358	3285764
32	0	1653000	0.0039	3389255	0	1553000	0	3491000	0.01	1453000	0.034	3291000
35	0	1653000	0.0022	3391000	0	1553000	0	3491000	0.009	1453000	0.024	3291000

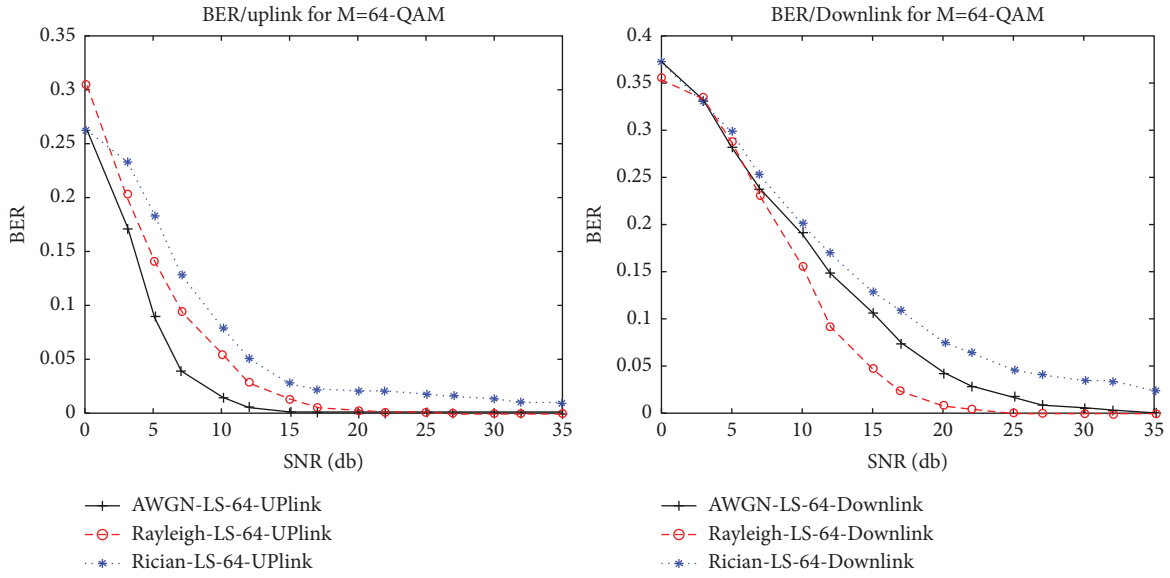


FIGURE 6: Comparison of the BER estimator performance for  $M=64$ -QAM across AWGN, Rayleigh, and Rician channels.

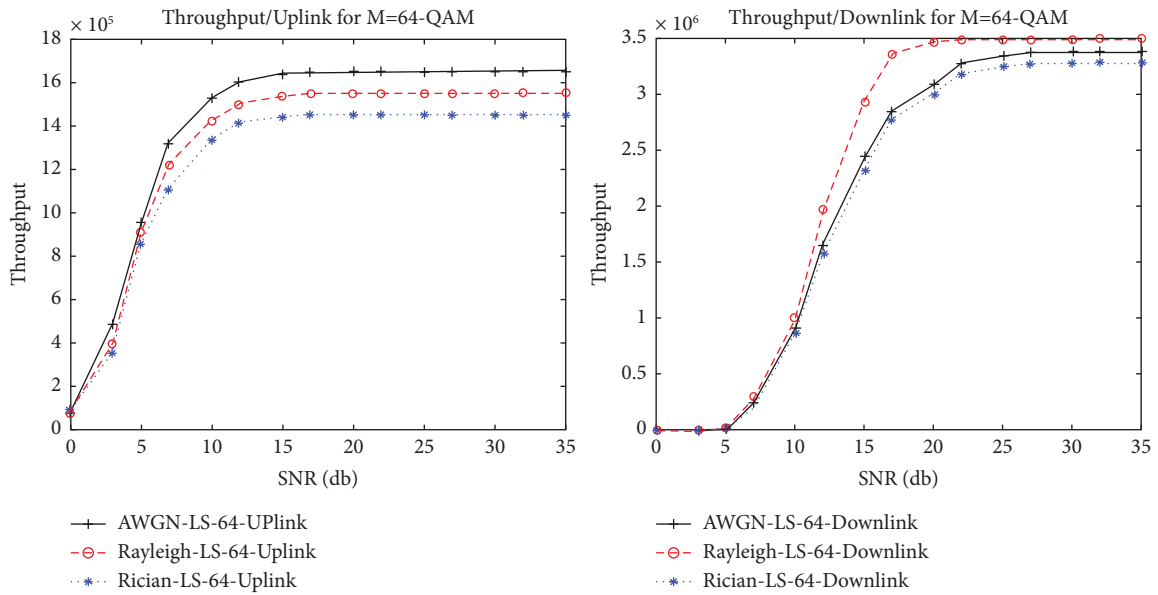


FIGURE 7: Comparison of LS estimators' throughput in a 64-QAM AWGN, Rayleigh, and Rician channels.

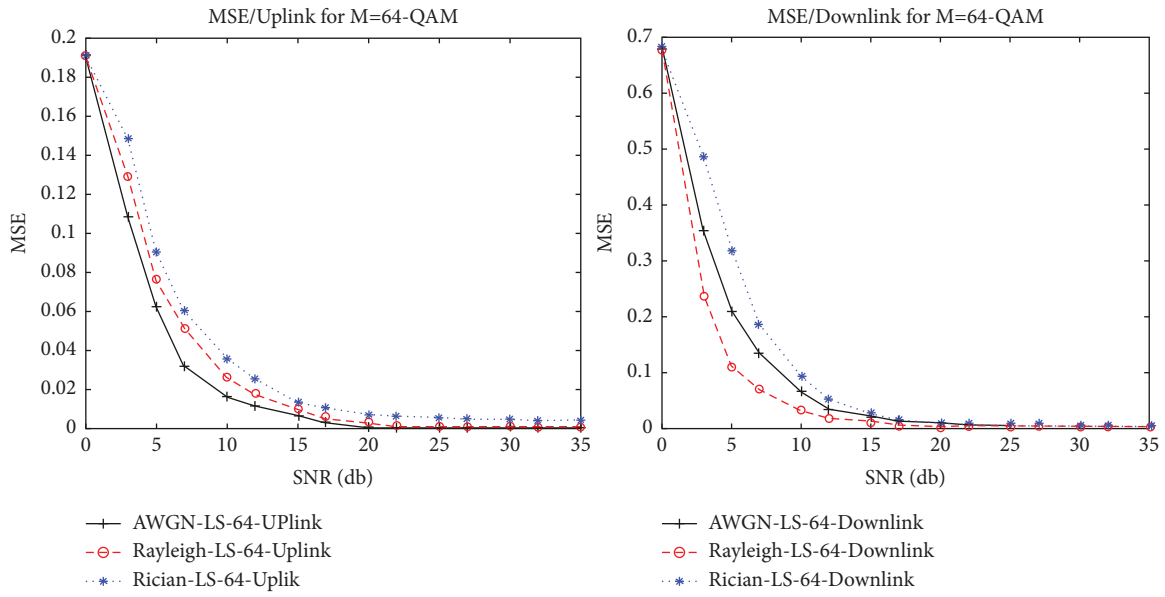


FIGURE 8: The performance of estimators' mean squared error (MSE) in AWGN, Rayleigh, and Rician channels for  $M = 64$ -QAM.

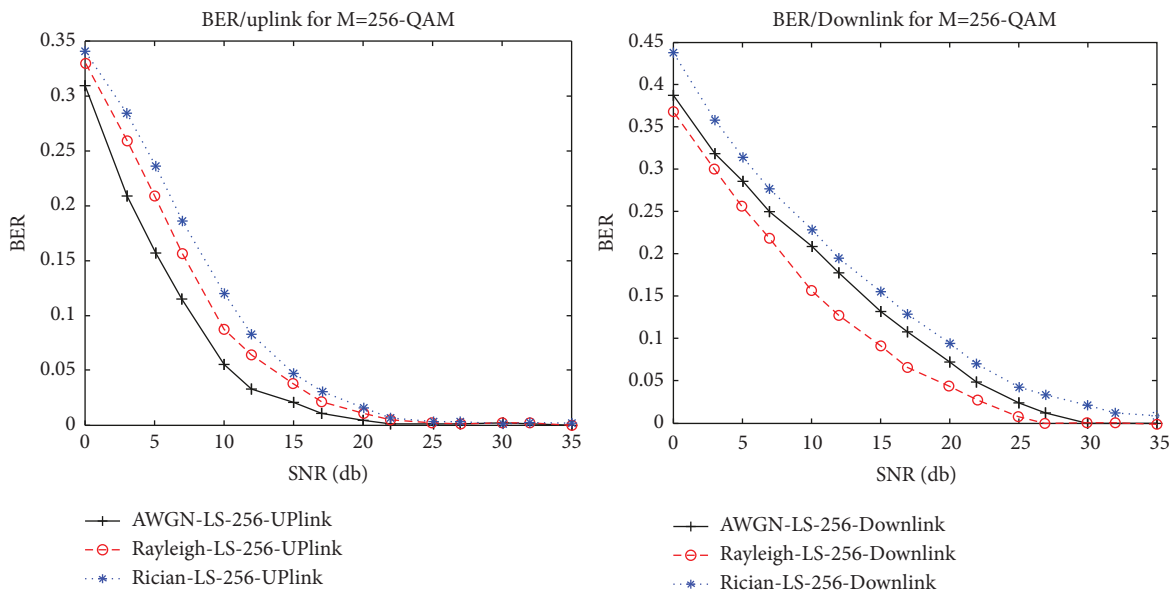


FIGURE 9: Comparing the BER estimator performance for  $M = 256$ -QAM across AWGN, Rayleigh, and Rician channels.

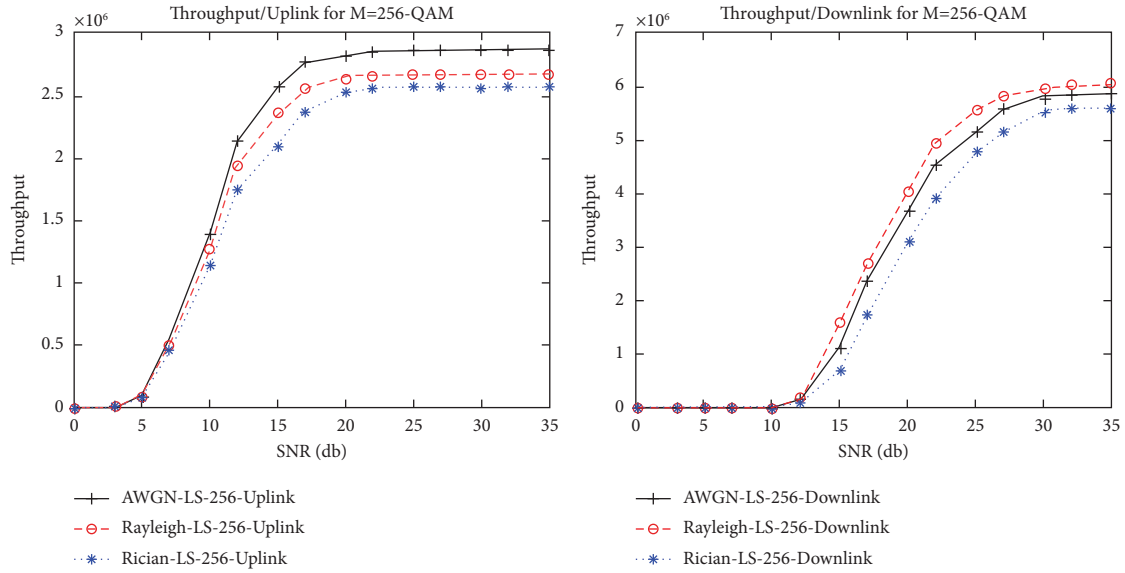


FIGURE 10: Comparison of LS estimators' throughput in 256-QAM AWGN, Rayleigh, and Rician channels.

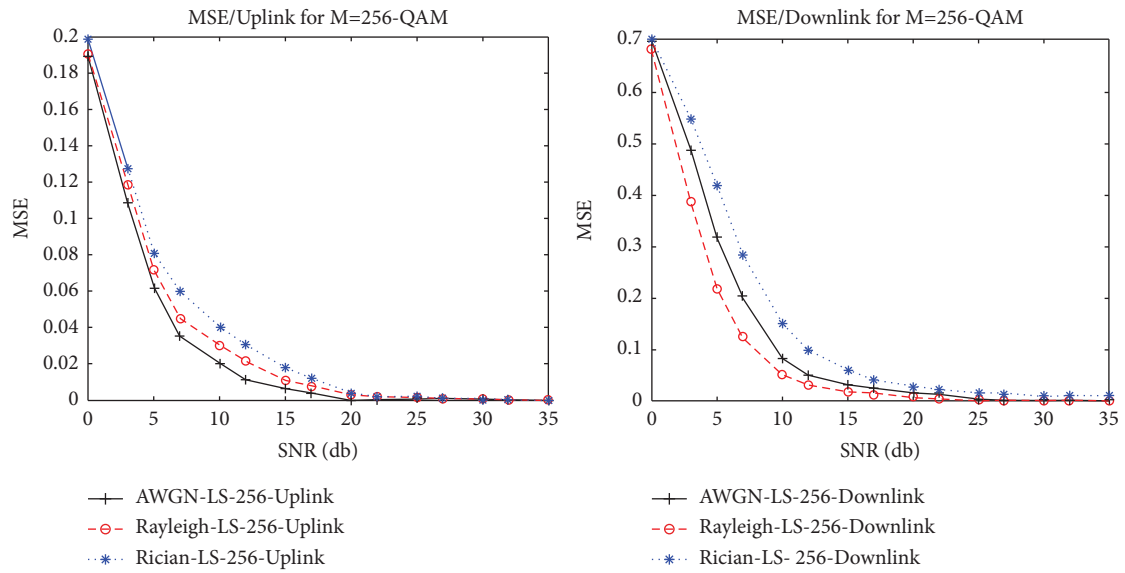


FIGURE 11: The performance of estimators' mean squared error (MSE) in AWGN, Rayleigh, and Rician channels for  $M=256$ -QAM.



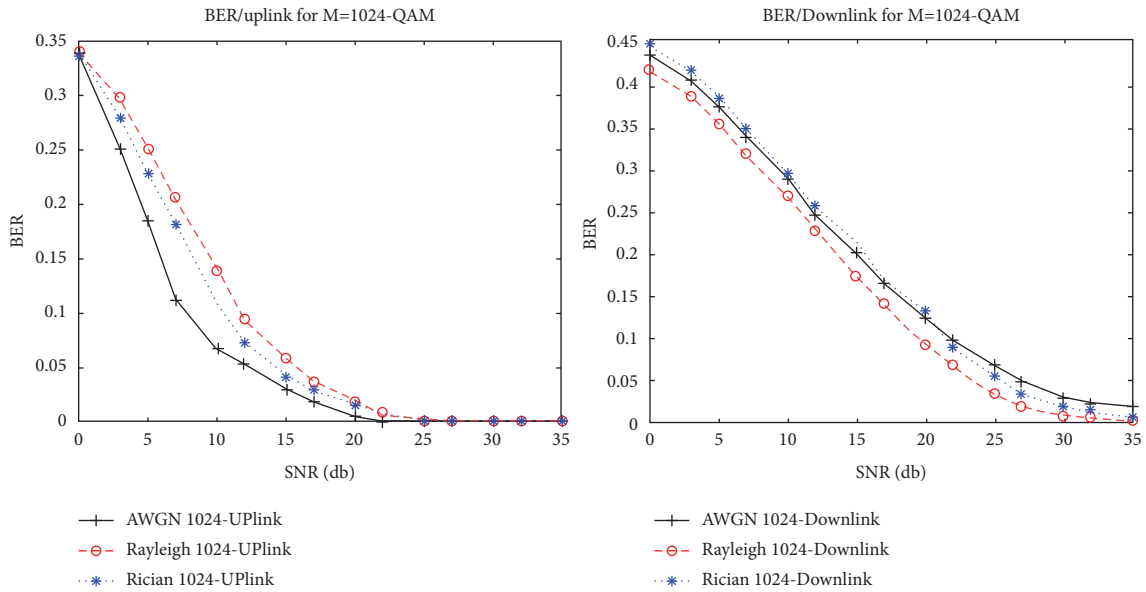


FIGURE 12: Comparison of the BER estimator performance for  $M = 1024$ -QAM across AWGN, Rayleigh, and Rician channels.

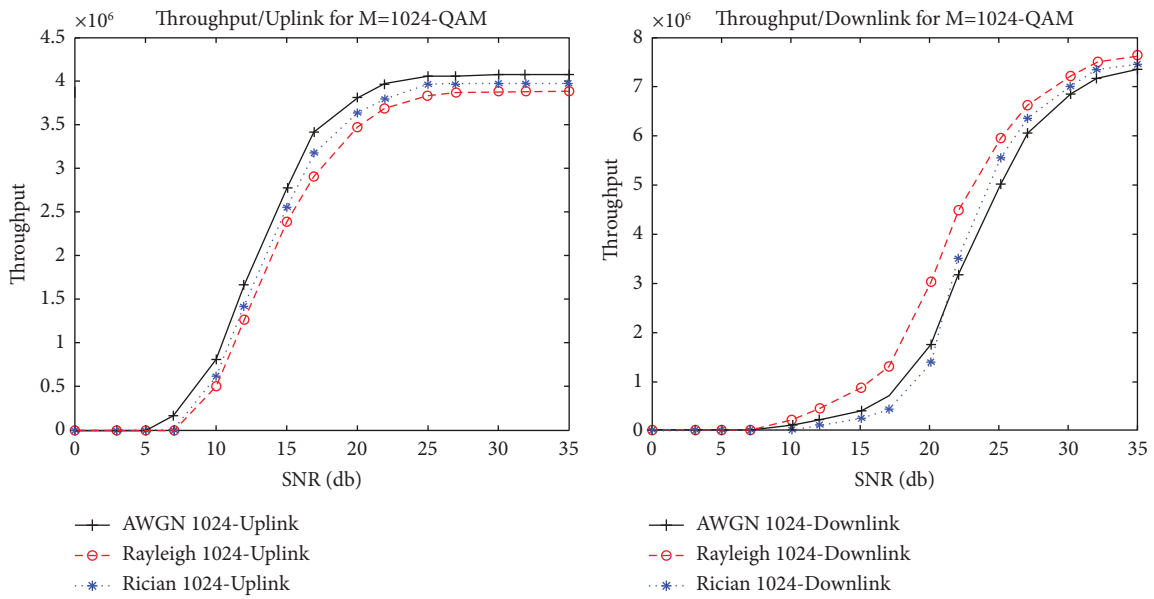


FIGURE 13: Comparison of LS estimators' throughput in a 1024-QAM AWGN, Rayleigh, and Rician channels.

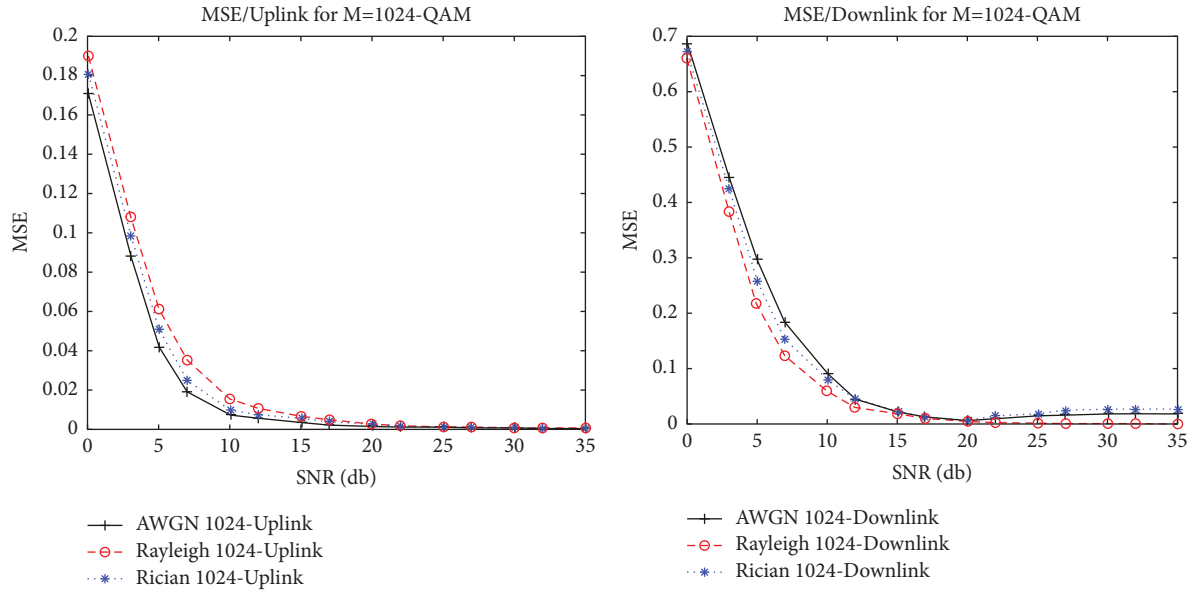


FIGURE 14: The performance of estimators' mean squared error (MSE) in AWGN, Rayleigh, and Rician channels for  $M = 1024$ -QAM.

maximum value which is 27 and the lowest value of BER 0.0003 for uplink and around 0.0119 for downlink and the throughput reach its maximum value in this case and the same happen for Rayleigh-LS as well as for Rician-LS. Then, the performance of the scenario will be different for those channels.

Figure 6 shows a comparison for BER estimator performance for uplink and downlink where  $M = 64$ -QAM across AWGN, Rayleigh, and Rician channels. In contrast, Figure 7 shows the comparison of the LS estimator according to throughput in 64-QAM, Rayleigh, and Rician channels for both uplink and downlink.

In Figure 8, the performance of the estimator comes with a comparison for all of the AWGN, Rayleigh, and Rician channels. According to mean squared error (MSE) for  $M = 64$ -QAM, we can notice that the value Rayleigh channel is the best performance compared to the other channels (AWGN and Rician).

The bit error rate against SNR with the value of  $M = 256$  for both uplink and downlink, Figure 9 shows a comparison for performance in different channel types AWGN, Rayleigh, and Rician. The result shows that the Rayleigh channel is better for downlink scenario due to the lower BER, while the AWGN channel is best for uplink scenario.

In Figure 10, the comparison comes for throughput against SNR (dB) in both uplink and downlink where  $M = 256$  QAM for AWGN, Rayleigh, and Rician channels.

We can notice from the curve that the value of throughput in downlink is the best for the Rayleigh channel and that is different for uplink where the AWGN channel overtakes the other channels. In Figure 11, the comparison come for MSE against SNR and it shows the performance for LS estimator in AWGN, Rayleigh, and Rician channels.

If we look forward at Figures 12–14, we can notice that the Rayleigh channel can give a worse performance in terms of BER, MSE, and throughput for all cases for  $M = 1024$ -QAM, and we compare this value with the same parameters according to AWGN and Rician in 1024-QAM for uplink. For downlink with  $M = 1024$ -QAM, as we can see, the Rayleigh show lower BER and MSE, and higher throughput than the AWG and Rician; as a result of all of these, Table 5 can show all the differences according to each value of BER and MSE which has been mentioned in all figures below and that will come out with different performances for LS estimators.

Table 6 shows a comparison between different values of SNR based on the channels' type: AWGN, Rayleigh, and Rician; we notice that the values of BER varied from 0.3392 to 0.0001 for uplink of AWGN and from 0 to 4098000 as a throughput; the comparison is different from one channel to others. Based on the simulation result, the best throughput we obtain is from the Rayleigh-LS channel.

TABLE 5: The performance of bit error rate (BER) and throughput (both uplink and downlink) for 256-QAM without channel estimation in AWGN, Rayleigh, and Rician, channels.

Channel SNR (dB)	AWGN-LS				Rayleigh-LS				Rician-LS			
	Uplink		Downlink		Uplink		Downlink		Uplink		Downlink	
	BER	Throughput	BER	Throughput	BER	Throughput	BER	Throughput	BER	Throughput	BER	Throughput
0	0.3096	0	0.3864	0	0.3295	0	0.3671	0	0.3404	0	0.4373	0
3	0.209	1435	0.3179	0	0.259	7175	0.299	0	0.2837	2870	0.3573	0
5	0.1568	83230	0.2851	0	0.2081	73275	0.2553	0	0.2359	61840	0.3148	0
7	0.1152	552475	0.2505	0	0.1559	503685	0.2177	0	0.1864	450995	0.2779	0
10	0.0561	1399125	0.2095	6059	0.0871	1271860	0.1583	12118	0.1197	1143160	0.2286	0
12	0.0324	2142455	0.1778	157534	0.0638	1932410	0.1277	193888	0.0834	1743890	0.1951	119357
15	0.0194	2564345	0.132	1118207	0.0384	2357170	0.091	1599709	0.0473	2105960	0.155	706089
17	0.0116	2772420	0.1082	2347783	0.0212	2553765	0.066	2699338	0.0307	2373855	0.1298	1747810
20	0.0051	2825515	0.0732	3662613	0.0109	2631255	0.0435	4020200	0.0154	2529820	0.0953	3098993
22	0.0015	2855650	0.049	4516905	0.004	2659955	0.028	4922938	0.0063	2558520	0.0711	3898755
25	0.0005	2868565	0.0243	5141009	0.0019	2670000	0.0082	5544038	0.003	2570000	0.0431	4762215
27	0.0003	2870000	0.0119	5574254	0.0019	2668565	0.0003	5810608	0.002	2568565	0.0347	5153047
30	0.0003	2870000	0.0009	5804496	0.0015	2670000	0.0003	5943906	0.002	2570000	0.0212	5519643
32	0.0001	2870000	0.0002	5825381	0.0008	2670000	0.0002	6010528	0.002	2570000	0.0133	5580233
35	0	2870000	0.0002	5846882	0.0005	2670000	0.0002	6028705	0.002	2570000	0.0079	5546882

TABLE 6: The bit error rate and throughput (both uplink and downlink) performance for 1024-QAM employing LS estimators in AWGN, Rayleigh, and Rician channels.

Channel SNR (dB)	AWGN-LS				Rayleigh-LS				Rician-LS			
	Uplink		Downlink		Uplink		Downlink		Uplink		Downlink	
	BER	Throughput	BER	Throughput	BER	Throughput	BER	Throughput	BER	Throughput	BER	Throughput
0	0.3392	0	0.4366	0	0.3398	0	0.4178	0	0.3373	0	0.4474	0
3	0.2505	0	0.4054	0	0.298	0	0.3869	0	0.2791	0	0.4165	0
5	0.1852	0	0.3749	0	0.2494	0	0.3548	0	0.2276	0	0.3848	0
7	0.1125	160700	0.3392	0	0.2067	11724	0.3189	0	0.1826	11724	0.3494	0
10	0.0673	809996	0.2889	109000	0.1392	505514	0.2691	209000	0.1073	608042	0.2968	10000
12	0.0531	1672054	0.2478	209000	0.0942	1266192	0.2294	450000	0.0734	1425158	0.2574	103000
15	0.0305	2787788	0.2027	375000	0.0591	2395604	0.1743	855000	0.0409	2558478	0.2138	240875
17	0.0192	3426054	0.1659	708875	0.0369	2922146	0.1423	1306500	0.0309	3200652	0.1711	400125
20	0.0055	3832486	0.1258	1756125	0.0192	3491452	0.0939	3045875	0.0156	3655934	0.1329	1388125
22	0.0009	4000530	0.0997	3182500	0.008	3712254	0.0689	4502125	0.0067	3810300	0.0915	3504125
25	0.0005	4068920	0.0706	5053125	0.0029	3865012	0.0356	5962375	0.0028	3976736	0.0568	5596375
27	0.0003	4092368	0.0504	6083375	0.001	3896276	0.0209	6644250	0.0012	3996276	0.0352	6388500
30	0.0002	4094092	0.0314	6859875	0.0005	3902138	0.0105	7234125	0.0004	3996046	0.0204	7034125
32	0.0003	4098000	0.0244	7205375	0.0002	3908000	0.0083	7520875	0.0002	3998000	0.0133	7363125
35	0.0001	4098000	0.0204	7372500	0.0001	3906046	0.0053	7660125	0.0001	3998000	0.0083	7489000

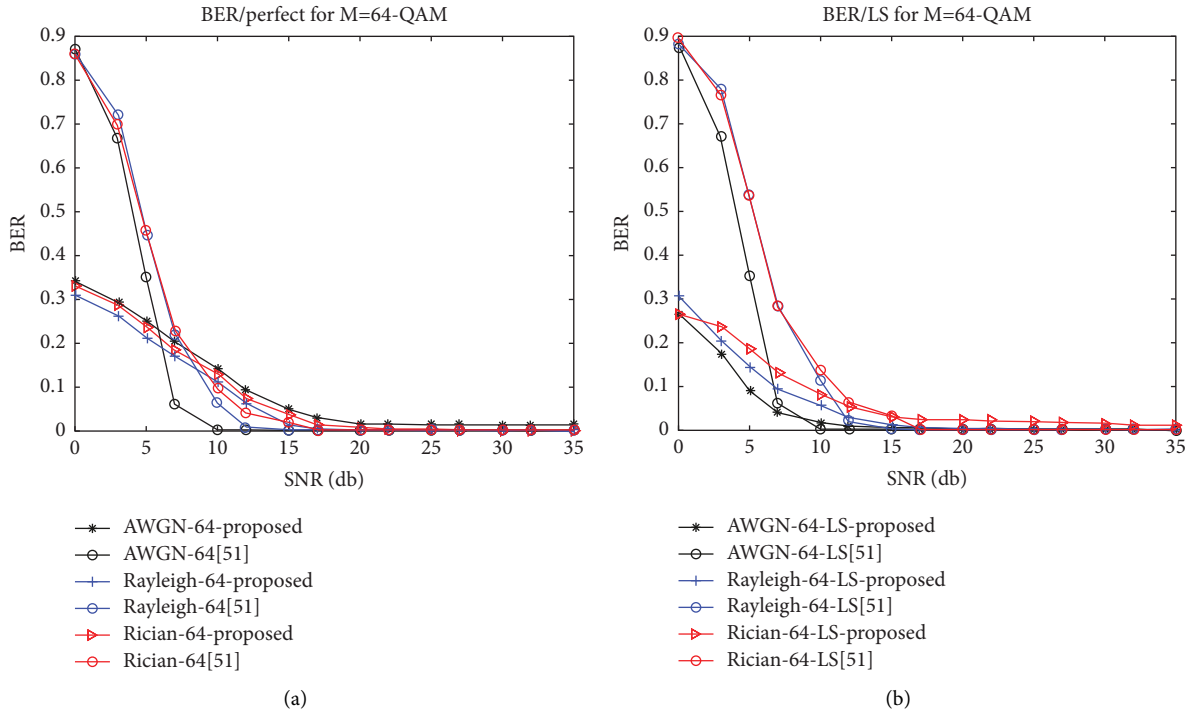


FIGURE 15: Illustration of the (a) BER performance without channel estimation and (b) BER performance of LS estimators in AWGN, Rayleigh, and Rician channels for 64-QAM.

Figure 15 shows that the BER performance before the channel was estimated and shows the performance for LS estimator in AWGN, Rayleigh, and Rician channels, where  $M = 64$  QAM and the proposed AWGN is the best performance for both (a) BER/perfect and (b) BER/LS.

## 10. Conclusions

This study thoroughly investigates multipath AWGN, Rayleigh, and Rician channel models. Utilizing 64-QAM modulation, the research evaluates the performance of an OFDM-MIMO system without channel estimation under these three channel conditions. In the uplink, simulation results reveal that the nonfading AWGN channel performs better than the Rayleigh and Rician fading channels, exhibiting a lower bit error rate. However, in the case of the Rician fading channel, the presence of a strong signal received through a direct line of sight enables it to achieve a better BER performance than the Rayleigh channel. We analyze how the LS estimator performs in Rayleigh, Rician, and AWGN nonfading channels with different modulation schemes, including 64-QAM, 256-QAM, and 1024-QAM. The investigation focuses on evaluating the bit error rate (BER), mean squared error (MSE), and throughput. As the signal-to-noise ratio increases, both the BER and MSE of the LS estimator decrease for both uplink and downlink scenarios across all modulation schemes. In future research, we plan to explore the capabilities of deep learning techniques, such as the super-resolution conventional neural network (SRCNN) and the denoising algorithm (DnCNN), in massive MIMO systems with RIS. The objective is to address

channel estimation challenges in cascaded channels and enhance BER and MSE performance.

## Data Availability

The data used to support the findings of this study are available from the corresponding authors upon request.

## Conflicts of Interest

The authors declare that they have no conflicts of interest.

## Authors' Contributions

W.H. conceptualized the study, was responsible for software and funding acquisition, was involved in study supervision and project administration, performed formal analysis and data curation, investigated the data, collected the resources, visualized the study, and prepared the original draft; W.H., H.K., A.F., and N.K. contributed to methodology; W.H., K.A., and N.K. validated the data; W.H., N.K., H.K., and A.F. reviewed and edited the manuscript. All authors have read and agreed to the published version of the manuscript.

## Acknowledgments

The authors thank the deanship of scientific research at the Northern Border University, Arar, KSA, for funding this research work through project number "NBU-FFR-2023-0043." The authors thank the Prince Faisal bin Khalid bin Sultan Research Chair in Renewable Energy Studies and Applications (PFCRE) at the Northern Border University for

their support and assistance. Also, the authors are grateful to the University Putra Malaysia Faculty of Computer and Communication Engineering and Iraq University College.

## References

- [1] A. Elnakeeb and U. Mitra, "Bilinear Channel estimation for MIMO OFDM: lower bounds and training sequence optimization," *IEEE Transactions on Signal Processing*, vol. 69, pp. 1317–1331, 2021.
- [2] H. Q. Ngo and E. G. Larsson, "Blind estimation of effective downlink channel gains in massive MIMO," in *Proceedings of the 2015 IEEE*, Santiago, Chile, December 2015.
- [3] V. V. Reddy and A. W. Khong, "Direction-of-arrival estimation of speech sources under aliasing conditions," in *Proceedings of the 2015 IEEE International Conference on Acoustics, Speech and Signal Processing (ICASSP)*, pp. 1–5, South Brisbane, Australia, April 2015.
- [4] A. Mezghani and A. L. Swindlehurst, "Blind estimation of sparse broadband massive MIMO channels with ideal and one-bit ADCs," *IEEE Transactions on Signal Processing*, vol. 66, no. 11, pp. 2972–2983, 2018.
- [5] M. X. Chang, "A new derivation of least-squares-fitting principle for OFDM channel estimation," *IEEE Transactions on Wireless Communications*, vol. 5, no. 4, pp. 726–731, 2006.
- [6] H. Minn, V. K. Bhargava, and K. B. Letaief, "A combined timing and frequency synchronization and channel estimation for OFDM," in *Proceedings of the 2004 IEEE International Conference on Communications (IEEE Cat. No.04CH37577)*, vol. 2, pp. 872–876, Paris, France, June 2004.
- [7] M. Imko, C. Mehlhrer, M. Wrulich, and M. Rupp, "Doubly dispersive channel estimation with scalable complexity," in *Proceedings of the 2010 International ITG Workshop on Smart Antennas (WSA)*, pp. 251–256, Bremen, Germany, February 2010.
- [8] X. He, R. Song, and W. Zhu, "Pilot allocation for sparse Channel Estimation in MIMO-OFDM systems," *IEEE Transactions on Circuits and Systems II: Express Briefs*, vol. 60, no. 9, pp. 612–616, 2013.
- [9] W. Zhou and W. H. Lam, "Channel estimation and data detection for OFDM systems over fast-fading and dispersive Channels," *IEEE Transactions on Vehicular Technology*, vol. 59, no. 3, pp. 1381–1392, 2010.
- [10] S. A. Ghauri, S. Alam, M. F. Sohail, A. Ali, and F. Saleem, "Implementation of OFDM and channel estimation using LS and MMSE estimators," *International Journal of Computer and Electronics Research*, vol. 2, no. 1, pp. 41–46, 2013.
- [11] B. Lin, C. C. Chang, Y. H. Tseng, J. R. Li, Y. S. Peng, and Y. K. Huang, "Using wireless near-infrared spectroscopy to predict wound prognosis in diabetic foot ulcers," *Advances in Skin and Wound Care*, vol. 33, no. 1, pp. 1–12, 2020.
- [12] H. Huang, J. Yang, H. Huang, Y. Song, and G. Gui, "Deep learning for super-resolution Channel Estimation and DOA estimation based massive MIMO system," *IEEE Transactions on Vehicular Technology*, vol. 67, no. 9, pp. 8549–8560, 2018.
- [13] H. He, C. Wen, S. Jin, and G. Y. Li, "Deep learning-based Channel Estimation for beamspace mmWave massive MIMO systems," *IEEE Wireless Communications Letters*, vol. 7, no. 5, pp. 852–855, 2018.
- [14] D. Neumann, T. Wiese, and W. Utschick, "Learning the MMSE channel estimator," *IEEE Transactions on Signal Processing*, vol. 66, no. 11, pp. 2905–2917, 2018.
- [15] S. Zhao, S. Yan, and J. Xi, "Bidirectional soft-decision feedback equalization for OFDM systems," *IEEE Wireless Communications Letters*, vol. 9, no. 8, pp. 1283–1286, 2020.
- [16] P. Schniter, "Low-complexity equalization of OFDM in doubly selective channels," *IEEE Transactions on Signal Processing*, vol. 52, no. 4, pp. 1002–1011, 2004.
- [17] C. Wen, W. Shih, and S. Jin, "Deep learning for massive MIMO CSI feedback," *IEEE Wireless Communications Letters*, vol. 7, no. 5, pp. 748–751, 2018.
- [18] S. Das and P. Schniter, "Max-SINR ISI/ICI-shaping multi-carrier communication over the doubly dispersive channel," *IEEE Transactions on Signal Processing*, vol. 55, no. 12, pp. 5782–5795, 2007.
- [19] E. Vlachos, A. S. Lalos, K. Berberidis, and J. Thompson, "Adaptive windowing for ICI mitigation in vehicular communications," *IEEE Wireless Communications Letters*, vol. 7, no. 6, pp. 974–977, 2018.
- [20] T. Wang, C. Wen, S. Jin, and G. Y. Li, "Deep learning-based CSI feedback approach for time-varying massive MIMO channels," *IEEE Wireless Communications Letters*, vol. 8, no. 2, pp. 416–419, 2019.
- [21] Tuwien, "Vienna 5G simulators," 2018, <https://www.tuwien.at/etit/tc/en/vienna-simulators/vienna-5g-simulators/>.
- [22] S. Coleri, M. Ergen, A. Puri, and A. Bahai, "Channel estimation techniques based on pilot arrangement in OFDM systems," *IEEE Transactions on Broadcasting*, vol. 48, no. 3, pp. 223–229, 2002.
- [23] Y. Li, L. J. Cimini, and N. R. Sollenberger, "Robust channel estimation for OFDM systems with rapid dispersive fading channels," *IEEE Transactions on Communications*, vol. 46, no. 7, pp. 902–915, 1998.
- [24] T. Hwang, C. Yang, G. Wu, S. Li, and G. Ye Li, "OFDM and its wireless applications: a survey," *IEEE Transactions on Vehicular Technology*, vol. 58, no. 4, pp. 1673–1694, 2009.
- [25] S. H. Sun, J. L. Hu, Y. Peng, X. M. Pan, L. Zhao, and J. Fang, "Support for vehicle-to-everything services based on LTE," *IEEE Wireless Communications*, vol. 23, no. 3, pp. 4–8, 2016.
- [26] F. J. Martin-Vega, B. Soret, M. C. Aguayo-Torres, I. Z. Kovacs, and G. Gomez, "Geolocation-based access for vehicular communications: analysis and optimization via stochastic geometry," *IEEE Transactions on Vehicular Technology*, vol. 67, no. 4, pp. 3069–3084, 2018.
- [27] H. Mao, H. Lu, Y. Lu, and D. Zhu, "RoemNet: robust meta-learning based Channel Estimation in OFDM systems," in *Proceedings of the ICC 2019 IEEE International Conference on Communications (ICC)*, pp. 1–6, Shanghai, China, May 2019.
- [28] F. J. Martin-Vega, I. M. Delgado-Luque, F. Blaquez-Casado, G. Gomez, M. C. Aguayo-Torres, and J. T. Entrambasaguas, "LTE performance over high speed railway channel," in *Proceedings of the 2013 IEEE 78th Vehicular Technology Conference (VTC Fall)*, pp. 1–5, Las Vegas, NV, USA, September 2013.
- [29] W. G. Jeon, K. H. Chang, and Y. S. Cho, "An equalization technique for orthogonal frequency-division multiplexing systems in time-variant multipath channels," *IEEE Transactions on Communications*, vol. 47, no. 1, pp. 27–32, 1999.
- [30] G. Li, H. Yang, L. Cai, and L. Gui, "A low-complexity equalization technique for OFDM system in time-variant multipath channels," in *Proceedings of the 2003 IEEE 58th Vehicular Technology Conference VTC 2003-Fall (IEEE Cat. No.03CH37484)*, vol. 4, pp. 2466–2470, Orlando, FL, USA, October 2003.

- [31] L. Rugini, P. Banelli, and G. Leus, "Simple equalization of time-varying channels for OFDM," *IEEE Communications Letters*, vol. 9, no. 7, pp. 619–621, 2005.
- [32] Y. Mostofi and D. C. Cox, "ICI mitigation for pilot-aided OFDM mobile systems," *IEEE Transactions on Wireless Communications*, vol. 4, no. 2, pp. 765–774, 2005.
- [33] X. Cai and G. B. Giannakis, "Bounding performance and suppressing intercarrier interference in wireless mobile OFDM," *IEEE Transactions on Communications*, vol. 51, no. 12, pp. 2047–2056, 2003.
- [34] M. B. Sutar and V. S. Patil, "LS and MMSE estimation with different fading channels for OFDM system," in *Proceedings of the 2017 International Conference of Electronics, Communication and Aerospace Technology (ICECA)*, vol. 1, pp. 740–745, Coimbatore, India, 2017, April.
- [35] P. V. Budhgaon, "Multipath fading channel modeling and performance comparison of wireless channel models," *International Journal of Electronics and Communication Engineering*, vol. 4, no. 2, p. 189, 2018.
- [36] A. F. Molisch, M. Toeltsch, and S. Vermani, "Iterative methods for cancellation of intercarrier interference in OFDM systems," *IEEE Transactions on Vehicular Technology*, vol. 56, no. 4, pp. 2158–2167, 2007.
- [37] S. Che and Y. Yang, "Low-complexity MMSE-SIC equalizer employing LDLH factorization for OFDM systems over time-varying channels," *IEEE Transactions on Vehicular Technology*, vol. 59, no. 8, pp. 4128–4131, 2010.
- [38] L. Rugini, P. Banelli, and G. Leus, "Low-complexity banded equalizers for OFDM systems in Doppler spread channels," *EURASIP Journal on Applied Signal Processing*, vol. 2006, no. 1, pp. 067404–71286, 2006.
- [39] T. W. Wu and C. D. Chung, "Correlatively precoded OFDM with reduced PAPR," *IEEE Transactions on Vehicular Technology*, vol. 65, no. 3, pp. 1409–1419, 2016.
- [40] H. G. Ryu, Y. Li, and J. S. Park, "An improved ICI reduction method in OFDM communication system," *IEEE Transactions on Broadcasting*, vol. 51, no. 3, pp. 395–400, 2005.
- [41] M. X. A. Chang, "A novel algorithm of inter-subchannel interference self-cancellation for OFDM systems," *IEEE Transactions on Wireless Communications*, vol. 6, no. 8, pp. 2881–2893, 2007.
- [42] K. Y. Lin, H. P. Lin, and M. C. Tseng, "An equivalent channel time variation mitigation scheme for ICI reduction in high-mobility OFDM systems," *IEEE Transactions on Broadcasting*, vol. 58, no. 3, pp. 472–479, 2012.
- [43] H. A. Le, T. Van Chien, T. H. Nguyen, H. Choo, and V. D. Nguyen, "Machine learning-based 5G-and-beyond channel estimation for MIMO-OFDM communication systems," *Sensors*, vol. 21, no. 14, p. 4861, 2021.
- [44] R. Chataut and R. Akl, "Massive MIMO systems for 5G and beyond networks—overview, recent trends, challenges, and future research direction," *Sensors*, vol. 20, no. 10, p. 2753, 2020.
- [45] C. Y. Ma, S. W. Liu, and C. C. Huang, "Low-complexity ICI suppression methods utilizing cyclic prefix for OFDM systems in high-mobility fading channels," *IEEE Transactions on Vehicular Technology*, vol. 63, no. 2, pp. 718–730, 2014.
- [46] H. Cheon and D. Hong, "Effect of imperfect channel information in OFDM-based WLAN," *Electronics Letters*, vol. 38, no. 16, p. 912, 2002.
- [47] S. H. Han and J. H. Lee, "An overview of peak-to-average power ratio reduction techniques for multicarrier transmission," *IEEE Wireless Communications*, vol. 12, pp. 56–65, 2005.
- [48] W. Zhang, X. G. Xia, and P. C. Ching, "Optimal training and pilot pattern design for OFDM systems in Rayleigh fading," *IEEE Transactions on Broadcasting*, vol. 52, no. 4, pp. 505–514, 2006.
- [49] European Telecommunications Standards Institute, *LTE; Evolved Universal Terrestrial Radio Access (E-UTRA); Physical Channels and Modulation; (3GPP TS 36.211 Version 16.4.0 Release 16): Technical Specification*, Sophia-Antipolis, Valbonne, France, 2021.
- [50] M. Morelli and U. Mengali, "A comparison of pilot-aided channel estimation methods for OFDM systems," *IEEE Transactions on Signal Processing*, vol. 49, no. 12, pp. 3065–3073, 2001.
- [51] M. A. Al-Dhahir, M. G. Al-Naffouri, and M. A. Al-Hajri, "Performance of MIMO-OFDM systems in Rayleigh fading channels with different numbers of transmit and receive antennas, and different modulation schemes," *IEEE Transactions on Wireless Communications*, vol. 21, no. 1, pp. 284–296, 2022.
- [52] S. Zhang, J. Zhang, and W. Chen, "Performance of MIMO-OFDM systems in rician fading channels with different values of the rician factor, and different antenna configurations," *IEEE Transactions on Vehicular Technology*, vol. 71, no. 4, pp. 2577–2589, April 2022.
- [53] M. R. D. Rodrigues, "Performance of MIMO-OFDM systems in AWGN channels with different values of the noise power," *IEEE Access*, vol. 10, pp. 123456–123467, 2022.
- [54] M. R. D. Rodrigues, A. A. F. A. Costa, and M. A. A. Costa, "Performance of MIMO-OFDM systems in block fading channels with different block lengths, and different Channel Estimation techniques," *IEEE Access*, vol. 10, pp. 11686–11697, 2022.
- [55] H. Liu, C.-K. Wen, and L.-C. Wang, "Performance analysis of MIMO-OFDM systems in nakagami fading channels with different values of the nakagami parameter, and different precoding techniques," *IEEE Transactions on Communications*, vol. 70, no. 8, pp. 3620–3630, 2022.
- [56] M. A. Al-Dhahir and M. G. Al-Naffouri, "Performance of MIMO-OFDM systems in log-normal fading channels with different values of the log-normal shadowing factor, and different power allocation schemes," *IEEE Transactions on Vehicular Technology*, vol. 71, no. 3, pp. 1736–1749, 2022.
- [57] S. Zhang, J. Zhang, and W. Chen, "Performance analysis of MIMO-OFDM systems in weibull fading channels with different values of the weibull shape parameter, and different diversity techniques," *IEEE Access*, vol. 10, pp. 84553–84564, 2022.
- [58] D. Bala, G. M. Waliullah, M. H. Rahman, M. I. Abdullah, and M. A. Hossain, "Analysis the performance of MIMO-OFDM for various modulation techniques over AWGN, Rayleigh fading and rician fading channel," *Journal of Network and Information Security*, vol. 9, no. 2, pp. 1–8, 2021.
- [59] J. van de Beek, M. Sandell, and P. Borjesson, "ML estimation of time and frequency offset in OFDM systems," *IEEE Transactions on Signal Processing*, vol. 45, no. 7, pp. 1800–1805, 1997.
- [60] G. H. Golub and C. F. Van Loan, *Matrix Computations*, The Johns Hopkins University Press, Baltimore, MD, USA, 3rd edition, 1996.
- [61] S. Sesia, I. Toufik, and M. Baker, *LTE-the UMTS Long Term Evolution: From Theory to Practice*, Wiley, Hoboken, NJ, USA, 2nd edition, 2011.